JOURNAL OF GEOPHYSICAL RESEARCH, VOL. 89, NO. A7, PAGES 5597-5612, JULY 1, 1984

Observations of the Dynamics of the Polar Thermosphere

P. B. HAYS,[1] T. L. KILLEEN,[1] N. W. SPENCER,[2] L. E. WHARTON,[2] R. G. ROBLE,[3] B. A. EMERY,[3] T. J. FULLER-ROWELL,[4] D. REES,[4] L. A. FRANK,[5] AND J. D. CRAVEN[5]

The dynamics of the polar thermosphere are examined by using observations made from the Dynamics Explorer 2 satellite. The results used in this study were obtained primarily from the Fabry Perot interferometer (FPI) and the wind and temperature spectrometer (WATS) during the time period from September 1981 through January 1982. Two primary geophysical conditions were examined: these were the southern summer and the northern winter polar regions. The results support the conclusion that above 60 degrees of latitude the neutral winds are strongly controlled by ion/neutral frictional momentum transfer resulting from magnetospheric convection. This implies that the natural coordinate system within which to display the neutral winds in the high polar thermosphere is magnetic. The collected observations of this study were used to assess the validity of two of the large thermospheric general circulation models. The result of this assessment was that the models reasonably represent the vector winds at high altitudes but do not, at present, accurately simulate the thermodynamics of that regime.

INTRODUCTION

The dynamics of the high-latitude thermosphere has been a source of conjecture throughout the past decade. The discussion began when satellite accelerometer [*De Vries*, 1972; *Wu et al.*, 1974] and early rocket chemical release observations of thermospheric winds [*Stoffregen*, 1972; *Meriwether et al.*, 1973; *Rothwell et al.*, 1974; *Kelley et al.*, 1977] showed variable, high-speed motions in the polar regions. The first reliable ground-based optical [*Hays et al.*, 1979] and radar [*Nagy et al.*, 1974] measurements of the thermospheric winds confirmed this complexity and clearly showed that the thermospheric wind field could not be modelled by simply using first-order solar tidal theory. The theoretical discussion began in a similar time frame with the classical paper of *Dickinson et al.* [1971] and with the first discussion of the high-latitude influence of ion convection by *Fedder and Banks* [1972]. Since these early contributions, there have been many significant advances in both the theoretical and the observational understanding of thermospheric dynamics and thermodynamics: these being summarized in several recent reviews [*Straus*, 1978; *Mayr et al.*, 1978; *Mayr and Harris*, 1979; *Rishbeth*, 1972, 1979; *Roble*, 1983]. However, there has been a tendency for the theoretical research to progress faster than the experimentalist can provide observational tests.

This paper provides a new set of observational dynamic and thermodynamic data obtained by the Fabry-Perot interferometer (FPI) [*Hays et al.*, 1981] and the wind and temperature spectrometer (WATS) [*Spencer et al.*, 1981], which are sampling the thermosphere from the Dynamics Explorer 2 spacecraft. The information provided by these instruments has been described in part in earlier discussions [*Killeen et al.*, 1982, 1983; *Spencer et al.*, 1982]. The particular data sets discussed here address two distinct temporal and spatial locations in the polar atmosphere. These are the southern summer region in October 1981, when the satellite was crossing the pole from 2100 hours to 0900 hours of local time (LT), and the northern winter region in December 1981, when the satellite was crossing the pole from 0600 hours to 1800 hours LT. During both of these time periods, there was extensive orbital coverage, providing a detailed survey of the variations in the polar thermosphere with universal time. This point is significant, and it will be shown that this coverage allows us to examine the influence of the magnetosphere-ionosphere coupling on the neutral atmosphere.

Based on this data set, a primary conclusion is that above 60 degrees of latitude the neutral winds in the high thermosphere are best described in a magnetic coordinate system. That is, the thermosphere wind system responds primarily to magnetospheric driving functions that map into the auroral region surrounding the magnetic poles of the earth. The most obvious of these forcing functions is the momentum source associated with the motion of ions that move in response to the polar convection electric fields, with a less obvious forcing being that caused by the Joule heating that accompanies the ion motion through the neutral gas. Both of these effects are enhanced when the auroral region is sunlit and the ionospheric density increased. This last influence is observed in both the seasonal and universal time behavior of the winds.

Rishbeth and Hanson [1974] have pointed out that the magnetospheric convection velocity is virtually divergence free, even if there are large spatial variations in the electric field. As a result of this property, *Rishbeth* [1977], *Mayr and Harris* [1978], and *Volland* [1979] have all shown that a "back pressure" does not seriously impede the winds driven by the ion drag momentum source at *F* region heights. Magnetospheric convection primarily drives a largely rotational, nondivergent, double-vortex system at these heights that lags the pattern of magnetospheric convection by a few hours. Joule heating, on the other hand, drives a divergent wind system that is primarily responsible for compositional and temperature changes [*Hays et al.*, 1973; *Mayr and Harris*, 1978; *Volland*, 1979].

One of the major questions of the past few years has been about the validity of the large numerical thermospheric general circulation models (TGCM's). Two of these models have been used to predict the response of the neutral atmosphere to the high-latitude magnetospheric input of energy and momentum [*Fuller-Rowell and Rees*, 1981; *Roble et al.*, 1982]. The final section of this paper compares in detail the averaged observational wind and temperature fields with those predicted by the NCAR TGCM [*Roble et al.*, 1982, 1983] and by the UCL TGCM [*Fuller-Rowell and Rees*, 1981]. The outcome of

[1]Space Physics Research Laboratory, University of Michigan.
[2]NASA/Goddard Space Flight Center.
[3]National Center for Atmospheric Research.
[4]Department of Physics and Astronomy, University College London.
[5]Department of Physics and Astronomy, University of Iowa.

Paper number 4A0141.
0148-0227/84/004A-0141$05.00

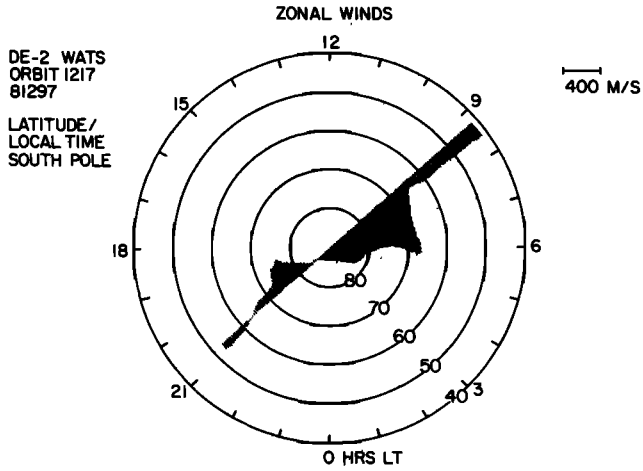

Fig. 1. Zonal neutral winds measured by the WATS instrument for the south pole pass on orbit 1217. The winds are plotted in geographic polar coordinates (geographic latitude and local solar time). The wind scale in m/s is indicated by the bar at upper right.

this comparison is that there is relatively good agreement between the general features of the observed wind fields and those of the models but that the observed temperature variations in the polar cap are larger than model predictions.

2. The Observations

The observations reported here were carried out from the Dynamics Explorer (DE 2) satellite by using the FPI and the WATS instruments. A detailed discussion of these instruments is given in the special issue of *Space Science Instrumentation* where the FPI [*Hays et al.*, 1981] and WATS [*Spencer et al.*, 1981] are described. The data analysis technique used to combine the meridional wind measured by the FPI and the zonal wind measured by the WATS is reviewed briefly below. A more complete description is given by *Killeen et al.* [1982].

2.1. *Zonal Wind*

The zonal wind and neutral gas kinetic temperature are measured with the WATS instrument by carefully occulting the orifice of a closed-source Massenfilter mass spectrometer with a small baffle. This baffle moves back and forth in front of the orifice, and the angle between the baffle center and the orifice center when the signal from the spectrometer is minimum determines the direction of motion of the thermospheric gas relative to the spacecraft. The temperature is determined from the angular width of the wake behind the baffle. The mass 28 peak (nitrogen) is used for the WATS measurement. It is assumed that the kinetic properties of nitrogen are representative of all thermally equilibrated neutral species. When the spacecraft motion is removed, the resultant velocity is the zonal component of the neutral atmospheric wind at the satellite. It should be noted that care must be exercised in the removal of the spacecraft velocity because of its large magnitude. The spacecraft attitude is known to within about 1 mrad (equivalent to 8 m/s) by on-board horizon and sun sensors, and the accuracy of these measurements has been confirmed independently by using a new star sensor [*Hays et al.*, 1981; W. B. Hanson, private communication, 1983]. The resulting zonal wind samples are referred to the position of the satellite as it moves through the orbit. In most cases the instrument is sufficiently sensitive to measure the zonal wind at altitudes below 600 km along the orbit. A representative data set is shown in Figure 1 for orbit 1217, where the DE satellite is passing through perigee near the southern geographic pole in October 1981. We note the rapid shearing of the zonal wind that is typical of the auroral regions.

2.2. *Meridional Wind*

The meridional wind and temperature of the neutral atmosphere are measured with the FPI instrument by determining the Doppler shift and width of naturally occurring thermospheric emission lines. The primary line of interest in the measurement of the meridional neutral wind is that emitted by $O(^1D)$ at wavelength 6300 Å. The lifetime of this metastable state (155 s) is sufficiently long to ensure complete thermalization before radiative deexcitation. The measured emission line profiles are therefore characterized by the ambient neutral temperature and bulk motion. The FPI measurement, by its nature, is remote from the spacecraft and provides a mean of the Doppler shift along the line of sight of the instrument weighted by the distribution of the $O(^1D)$ atoms. Usually, the principal contribution to the Doppler shift comes from a narrow region centered on the point at which the line of sight is parallel to the surface of the earth. Thus the meridional wind measured by the FPI is always ascribed to that point, and consequently, as the spacecraft moves through its orbit and the line of sight is oscillated up and down on the horizion, the meridional wind is measured as a function of altitude and latitude below and ahead of the satellite. This implies a slight time shift between the measurements of the two components of the wind. During the daytime period and in the auroral zone, where there is sufficient light emitted by the atmosphere, the meridional wind and temperature can be measured throughout a region extending from 225 km below the spacecraft to the orbital altitude. This is true as long as the tangent point of the line of sight is below 600 km. A good illustration of this is seen in Plate 1, where altitude profiles of the meridional wind, temperature, and brightness of the 6300-Å emission are shown in a band below the spacecraft on orbit 1200. There is little uncertainty in these measurements as a result of the spacecraft orientation, since the line-of-sight direction is along the spacecraft velocity vector. The major errors are statistical, and the magnitude of this uncertainty can be seen in the granularity in the color map. We note here that the positive sense to the wind is in the direction of the satellite motion, here shown in yellow. It should also be noted that the true anomaly of the orbit is designated here as the angle along the track (AAT) and will be used as such throughout this paper. One observes, as with the zonal wind, that the thermospheric temperature and meridional wind speeds are high and variable in regions associated with the auroral zones.

2.3. *Vector Wind Fields*

The horizontal wind vector in the upper thermosphere can be determined along the track of the DE spacecraft by combining the measurements of WATS and FPI [*Killeen et al.*, 1982]. We note that the FPI measurements are selected to be those made at the satellite altitude to be compatible with the WATS "in situ" zonal wind component. This process is completed for much of the DE data base where both instruments are in the proper modes of operation. Here we present two sets of these data obtained in October and December 1981 when the spacecraft was passing through perigee in the southern summer and northern winter polar regions. There are obviously three parameters in addition to altitude that must be important in determining the wind: these being local time,

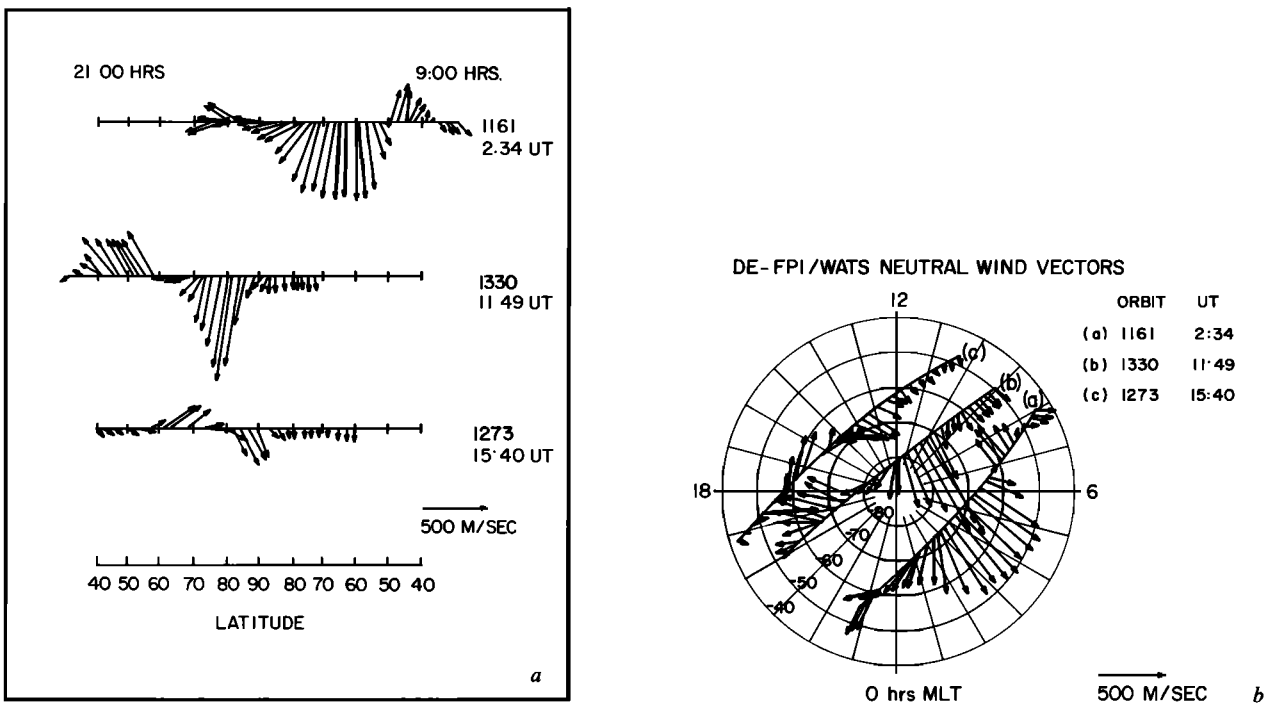

Fig. 2. (*a*) Neutral wind vectors plotted along the track of DE 2 for several south pole passes. The satellite crosses the pole from 2100 LT to 900 LT, and the vectors are plotted with respect to this local time plane (LT increases in anticlockwise direction). (*b*) Wind vectors from the same orbits plotted in geomagnetic (centered dipole) polar coordinates (geomagnetic latitude and magnetic local time).

latitude, and universal time or geographic longitude. These parameters are important, since they must be used to order the data taken from any one time period. It is evident that local time as well as the season is fixed by the satellite orbit and will only vary slowly as the orbit precesses [*Hoffman et al.*, 1981]. Thus in the presentation of the wind vectors measured along the satellite track for a period of the order of a month or shorter we are primarily observing the universal time and latitude variations for situations where the local time period and season are unchanging.

Plate 2 shows a northern polar projection of orbit 1840 (December 5, 1981) with the total wind vectors from the FPI and WATS measurements superimposed on an auroral image taken by the scanning auroral imager (SAI) [*Frank et al.*, 1981] on the high-altitude DE spacecraft during the same time period. The auroral image is taken in the 131-nm wavelength region. The red on the right of the image is the day, and the upper portion of the auroral oval is the evening sector. The transpolar wind flowing from the day toward the night is clearly seen [*Meriwether et al.*, 1973], as is the strong reversal to sunward winds in the evening sector of the auroral zone found in the Alaskan results of the Michigan Airglow Observatory [*Nagy et al.*, 1974; *Hays et al.*, 1979]. Thus a clear relationship is demonstrated between the vector wind pattern and the auroral oval, which is a strong indication that the polar winds will be ordered in a coordinate system centered on the magnetic pole. This tendency will be demonstrated often in the results from the DE mission where a strong universal time modulation in the neutral dynamics is evident.

A series of wind vector projections are shown in Figure 2*a* for a number of orbits crossing the southern polar region in October 1981. These orbits are selected such that they represent an evenly distributed series of universal times, thus crossing the southern auroral oval in quite different regions. One should note the significant differences in the vector wind fields on these different orbits, all of which follow the same path in local time and geographic latitude. The same orbits of data are shown in centered dipole magnetic coordinates in Figure 2*b*, and the ordering is vastly improved. Here the wind field shows the transpolar jet and the reversal in the evening auroral oval described in the previous discussion.

The northern polar region as shown in Plate 2 illustrates the same tendencies as its southern counterpart. Figure 3*a* shows a series of wind measurements taken along orbits distributed in universal time in December 1981. We note again that there are significant differences in these data when ordered in geographic coordinates. The same information shows a much clearer pattern when presented in a dipole magnetic coordinate system centered on the northern dipole as seen in Figure 3*b*. The geographic disorder is not so dramatic in the northern polar region, since the separation of the geographic pole and the magnetic pole is smaller than that in the south. It will be shown later that the temperatures measured in both polar regions show the same magnetic ordering as the winds.

2.4. *Average Wind Fields*

The previous discussions of individual orbits of data obtained over the full range of universal time indicates that one might expect a clear picture of the dynamics to emerge from averaging data by universal time. This was done with both components of the wind and the kinetic temperature measured by FPI for the October southern polar passage and for the December northern polar passage.

(*a*) *Southern summer polar region.* The data set used to produce the averaged behavior of the winds and temperature over the southern pole was, in most cases, the same for zonal

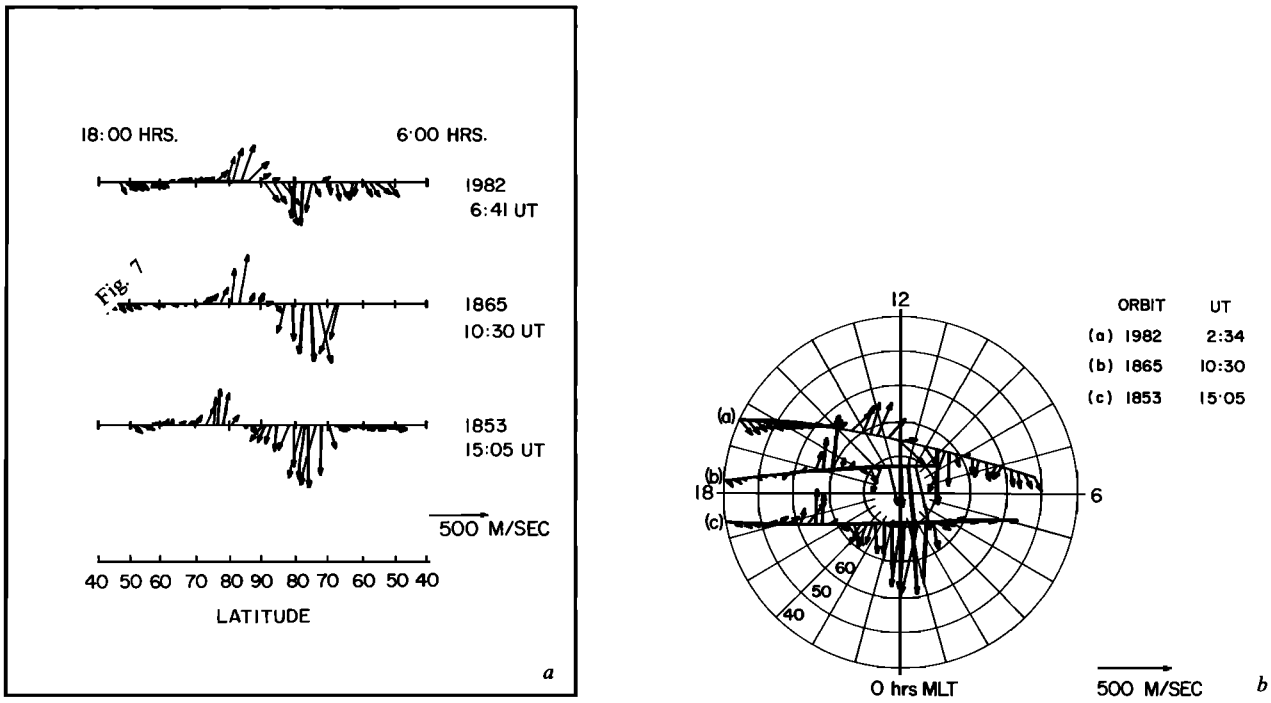

Fig. 3. (*a*) Neutral wind vectors plotted along the track of DE 2 for several north pole passes. The satellite crosses the pole from 1800 LT to 600 LT, and the vectors are plotted with respect to this local time plane (LT increases in anticlockwise direction). (*b*) Wind vectors from the same orbits plotted in geomagnetic (centered dipole) polar coordinates (geomagnetic latitude and magnetic local time).

wind as for the meridional wind and temperature. However, in some cases, additional data could be added to one or the other average when either FPI or WATS was in a mode of operation suitable for wind measurements while the other was in an unsuitable mode. The FPI meridional wind and temperature maps contained 58 orbits of data taken between orbits 1050 and 1374, while the WATS zonal wind average was made up of 34 orbits of data obtained in the same time period. The wind data set is the same as that used by *Killeen et al.* [1983] in our first investigation of the average high-latitude wind field.

The averaged zonal wind is presented in Plate 3*a*, where the vertical scale is the AAT measured from the equatorial crossing, and the horizontal scale is universal time. The averages were carried out in 5° angular bins and 2-hour universal time bins. The white line crossing the figure is the projection of the magnetic pole on the orbital track. Here the magnitude of the zonal wind is mapped in color, with yellow corresponding to a 200 m/s wind directed toward the right of the spacecraft and black to a 600 m/s wind to the left. We note the strong universal time dependence of the zonal wind and the fact that the dependence follows the projection of the magnetic pole on the orbit. The zonal component of the wind shows a strong tendency to blow from day toward night just before the spacecraft passes the magnetic pole, with flow from night to day observed near 0000 and 1200 hours UT. This pattern is seen on individual orbits as well as in the average and thus is a permanent feature of the circulation pattern.

The averaged meridional wind is shown in Plate 3*b*, where the same horizontal and vertical scales are used as for the zonal wind. The color coding is different in this case: yellow being a meridional wind of 300 m/s in the direction of the spacecraft motion (here from night to day) and black being a 500 m/s wind toward the night. One should recall that the night portion of the orbit is at 2100 LT and the day portion at 0900 hours. We note again the strong universal time dependence of this wind component. The meridional wind map shows two distinct regions: one between 0200 and 1200 hours UT, where the motion is from day to night, and a second where the flow is from night to day. Both of these regions closely follow the magnetic polar projection shown as the white line on this figure.

The interpretation of these results is simplified by examining Plate 3*c*, where a Heppner model ionospheric convection pattern [*Heppner*, 1977] is superimposed on a geographic southern polar projection of the orbit at four universal times. If one assumes that the neutral atmosphere responds locally to the ionospheric convection, one can use these diagrams to interpret our wind patterns. Quite clearly from these projections one would expect from 0300 to 0900 hours that both the zonal and meridional wind pattern should remain relatively constant in shape but that they would shift toward the night as the ionospheric convection pattern translates toward the night. A similar situation exists in the 1500 to 2100 hours time period where the pattern is shifting from night to day, with the orbit passing tangent again to the convection pattern along the afternoon auroral oval. A sharply contrasting behavior is expected in the UT periods between 0900–1500 and 2100–0300 hours. During these periods, the orbital path progresses directly across the entire polar convection pattern, so that here a sequence of rapid changes in the winds observed by the satellite would be expected on successive orbits. The neutral circulation does indeed follow the ion convection pattern, particularly over the polar cap and the dusk auroral zone. The wind pattern shifts parallel to the orbit in the 0300–0900 and 1500–2100 hours periods as expected.

These averaged results for the meridional and zonal winds can now easily be reformatted into a map of the averaged wind vector field observed along the track of the spacecraft over the southern summer polar region. Plate 5*a* shows the averaged vector wind field superimposed on the averaged temperature field measured by the FPI in the southern early summer. Here the format is identical to that used in the previous average maps. The vector winds exhibit the same general features described for the components, but there is a clear difference in the two transition regions. That is, one would expect that the 0900–1500 hours period would be a mirror image of the 2100–0300 hours period if the polar winds were driven by an unchanging ion convection pattern in an unchanging ionosphere. However, it is clear that the ionosphere is more fully developed (i.e., larger electron densities) near the 2400 hours UT time, when the magnetic pole is displaced toward the sun, than in the 1200 hours time when the magnetic pole is in darkness. Thus we find that the neutral winds do indeed respond strongly to the ion convection as a forcing function but that there is a modulation of the response that depends on the development of the ionosphere. There is no clear picture formed by the neutral temperature map, with the exception that the polar region is warmer than the low-latitude regions. The polar cusp does appear in the temperature at 0100 and 1300 UT as an enhancement on the dayside of the magnetic pole. The temperature results do show significant variances with magnetic activity that are discussed in detail in a forthcoming paper (T. L. Killeen et al., manuscript in preparation, 1984).

(*b*) *Northern winter polar region.* The data set used to produce the averaged behavior of the winds and temperature over the northern pole was treated in the same manner as southern data. The FPI meridional wind and temperature maps contained 98 orbits of data taken between orbits 1795 and 2125, while the WATS zonal wind average was made up of 22 orbits of data obtained in the same time period.

The averaged zonal wind is presented in Plate 4*a* for the northern winter polar region where the scaling is the same as that used for the southern data. Here the magnitude of the zonal wind is mapped in color, with yellow being 200 m/s wind to the right of the spacecraft, which is toward the day, and black being an 800 m/s wind to the left, or night. The strong universal time dependence of the zonal wind and the fact that the dependence follows the projection of the magnetic pole on the orbit is again obvious. Over the polar cap, the zonal component of the wind always is from day to night, as shown in this figure in the dark region that follows the projection of the magnetic pole onto the orbit. A wind reversal to sunward is observed when the orbit crosses the evening auroral oval, seen here as the yellow region of flow toward the day above the transpolar flow described above. There is little evidence for such a strong reversal in the morning. These tendencies were seen earlier on individual orbits and are shown here to be regular features of the circulation pattern.

The averaged meridional wind is shown in Plate 4*b*, where the same horizontal and vertical scales are used as for the zonal wind. The color coding is different here: yellow being a meridional wind of 200 m/s in the direction of the spacecraft motion, toward evening, and black being a 200 m/s wind opposite to the spacecraft motion, toward morning. We note again the strong universal time dependence of this wind component. The meridional wind map shows two distinct regions, a convergence in the wind before 1200 hours UT and a general divergence after that time. Both of these regions closely follow the magnetic polar projection shown as the white line on this figure.

The interpretation of these results is simplified by examining Plate 4*c*, where we again use a model ionospheric convection pattern [*Heppner*, 1977, model A] to illustrate the relationship between the ion motions and the neutral dynamics. We make the assumption that the neutral atmosphere responds locally to the ionospheric convection and attempt to explain the observed wind patterns by using the model convection pattern. From these projections one would expect that from 0300 to 0900 hours both the zonal and meridional wind pattern should remain relatively constant but would shift further toward morning as the ionospheric convection pattern translates parallel to the twilight line. One should note in this time period that the orbit is passing through or near to the polar cusp. During this period, there is a clear convergence in the meridional winds associated with the convergence in the ion convection pattern near the cusp. A similar situation exists in the 1500 to 2100 hours period where the convection pattern is displaced toward the dayside but shifts parallel to the orbit as time progresses. Here the orbit tends to bisect the polar cap with a bias toward the night side but never crosses over the midnight sector of the auroral oval. The meridional wind shows the influence of the ion convection pattern, following the divergent flow of the ions occurring near the Harang discontinuity. Contrasting behavior is expected in the 0900 to 1500 and the 2100 to 0300 hours UT periods where one observes the orbital path translating across the convection pattern from the cusp region toward the midnight polar cap. Since the northern polar passage is parallel to the twilight line, we do not expect or observe differences in these two polar transits. Throughout, one observes that the zonal winds show strong transpolar flow over the polar cap when the spacecraft is near the magnetic pole and that there is a dayward flow in the evening sector after crossing the polar cap. These two characteristics are clearly seen in the blue and yellow color bands on Plate 4*b* that parallel the white pole projection line. The neutral wind pattern again demonstrates a strong relationship to the ion convection pattern.

These averaged results for the meridional and zonal winds are now reformatted into a map of the averaged wind vector field observed along the track of the spacecraft over the northern winter polar region. Plate 6*a* shows the averaged vector wind field superimposed on the averaged temperature field measured by the FPI in the northern auroral zone. The format used here is identical to that used in the previous average maps. One again observes the strong magnetic ordering of the neutral dynamic field, with a very marked temperature maximum over the polar cap and at the cusp. There is, in addition to the polar cap temperature maximum, a significant minimum in the thermospheric temperature in the vicinity of the early evening crossing of the auroral oval. This strong minimum in temperature, approximately 300 K less than the polar cap, is seen as the dark region above the polar projection near 1200 and 2400 hours UT. This temperature minimum is associated with the dayward flow of neutrals and ions that occurs in the evening sector of the auroral oval. The convergence in the wind near the polar cusp is seen in the 0300 to 0900 hours UT period as expected, and the divergence in the midnight sector is apparent in the 1500 to 2100 hours period. The high temperatures in the polar cap are associated with the high transpolar winds, with the temperature maximum being seen near the cusp.

We speculate that the high temperature over the polar cap

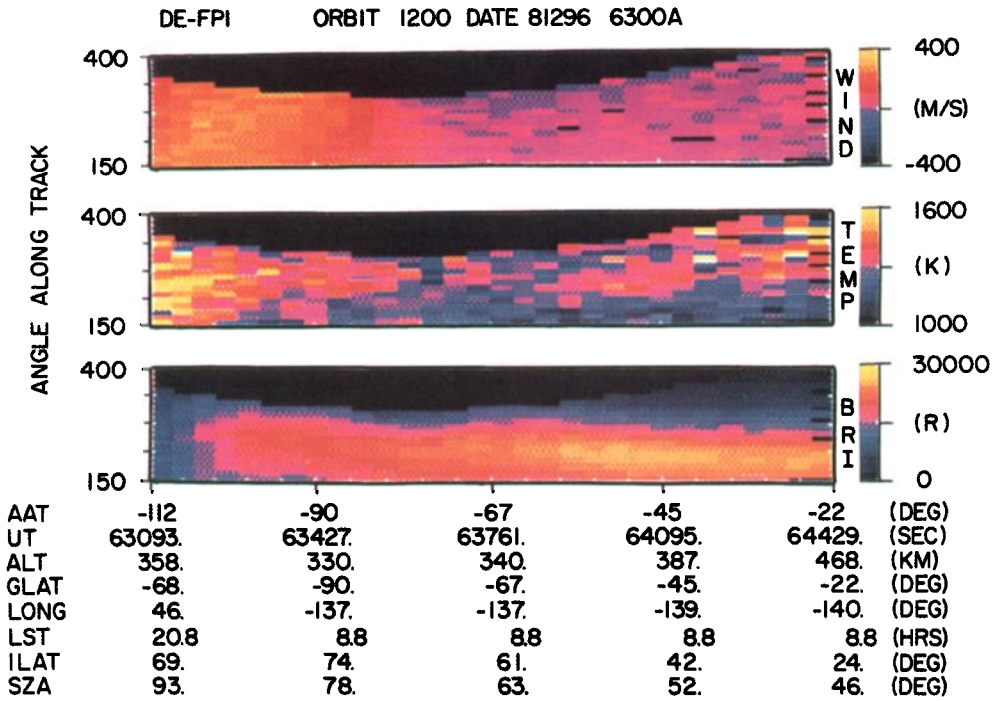

Plate 1. Color-coded plots of the geophysical observables of the FPI instrument for orbit 1200. In the top panel, measured meridional neutral winds (m/s) are plotted as a function of altitude of the tangent point along the FPI line of sight and UT. A positive wind is one that blows in the direction of the spacecraft velocity. The middle panel shows measured temperatures (K), and the bottom panel shows line-of-sight surface brightnesses (Rayleighs). All abscissae refer to satellite coordinates at the moment the spacecraft flies over the appropriate tangent point. AAT is the angle along the track which varies from $-180°$ to $+180°$ with zero at the equator.

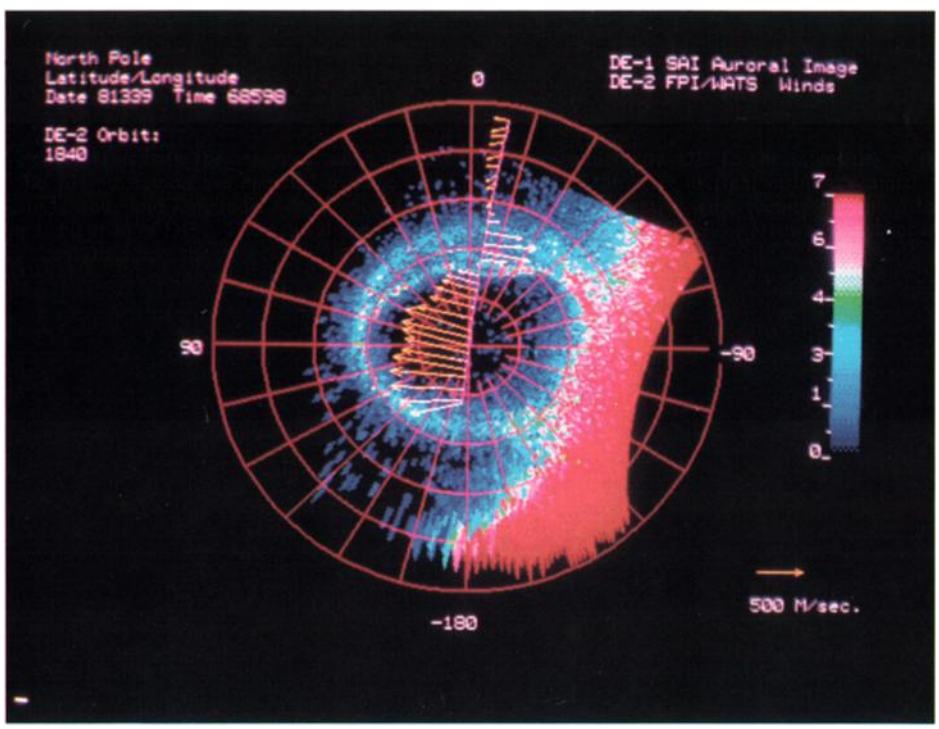

Plate 2. Image taken with the scanning auroral imager (SAI) instrument on DE 1. The intensities of the auroral emission in the 131-nm region are encoded in false color according to the scale at right (arbitrary units). The polar coordinates are latitude and longitude. Superimposed on the image are the neutral wind vectors measured by FPI and WATS during orbit 1840 of DE 2. The neutral wind measurements are given by the yellow arrows. Note that the twilight line is seen on the right side of the image.

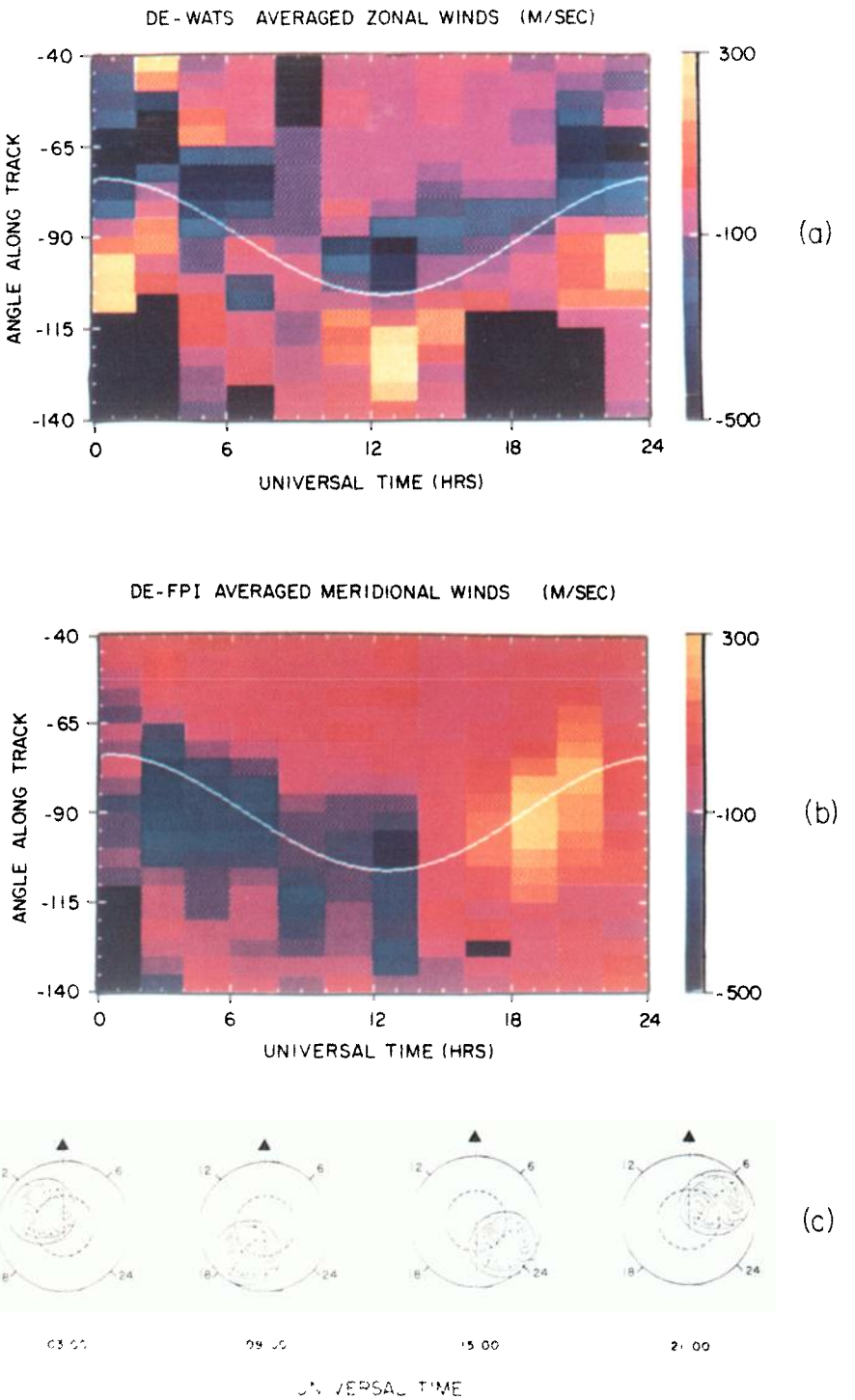

Plate 3. (*a*) Averaged zonal winds measured by WATS for the south pole passes of DE 2 in October 1981. The winds are color coded according to the scale at right (positive to the right of the spacecraft). The data are plotted with angle along the track of the spacecraft and in universal time. The white line represents the locus of the projection of the magnetic pole onto the plane of the orbit. (*b*) Averaged meridional winds measured by FPI for the south pole passes during October 1981 plotted in a similar manner. The meridional winds are color coded according to the scale at right with positive in the direction of the satellite velocity. (*c*) Polar dials (southern latitude and local solar time) showing the relative geometry, at four different universal times, of the track of the spacecraft (ascending vertical arrow) and the ion convection patterns, here represented by the empirical model of Heppner (see text).

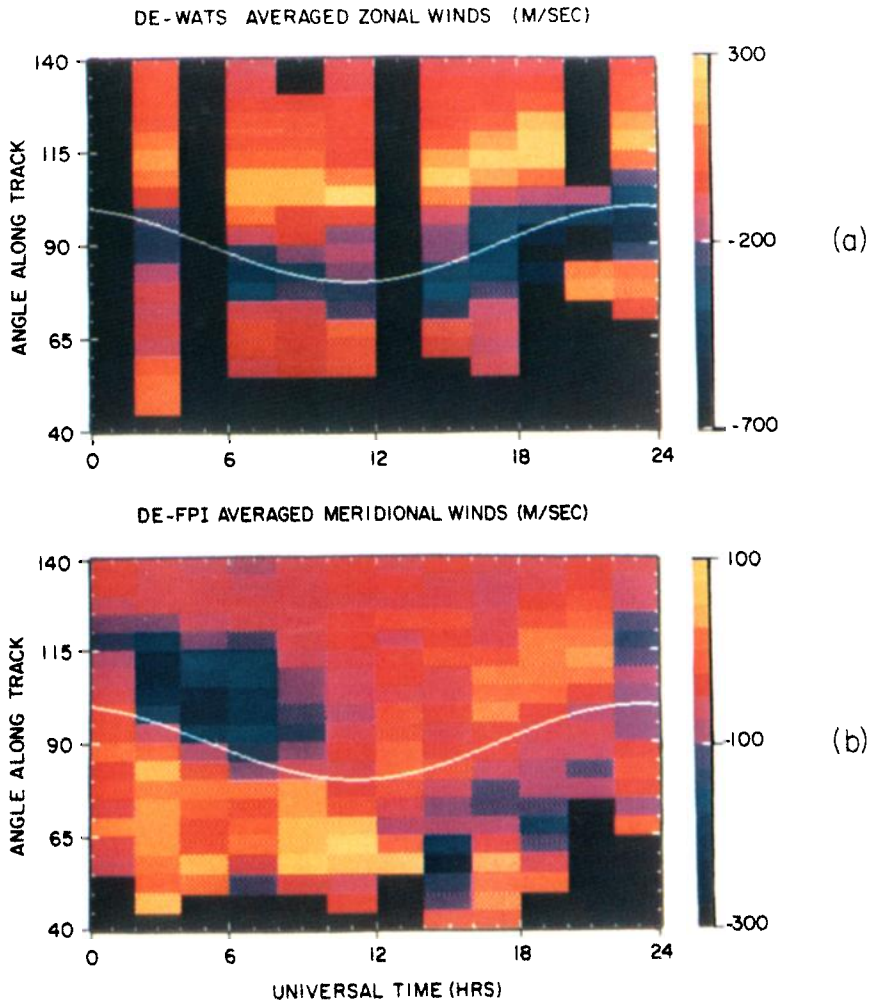

Plate 4. (*a*) Averaged zonal winds measured by WATS for the north pole passes of DE 2 in December 1981. The winds are color coded according to the scale at right (positive to the right of the spacecraft). The data are plotted with angle along the track of the spacecraft and in universal time. The white line represents the locus of the projection of the magnetic pole onto the plane of the orbit. (*b*) Averaged meridional winds measured by FPI for the north pole passes during December 1981 plotted in a similar manner. The meridional winds are color coded according to the scale at right with positive in the direction of the satellite velocity. (*c*) Polar dials (northern latitude and local solar time) showing the relative geometry, at four different universal times, of the track of the spacecraft (ascending vertical arrow) and the ion convection pattern, here represented by the empirical model of Heppner (see text).

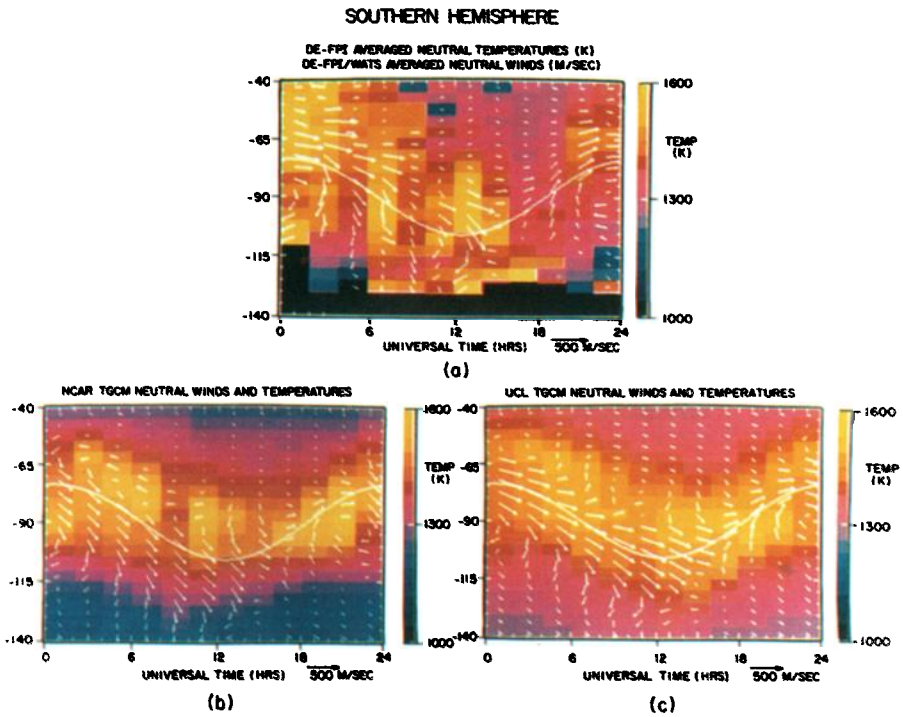

Plate 5. Comparison of the measured and predicted behavior of the thermospheric dynamics and thermodynamics for the summer (south) pole study. (*a*) Measurements of the average neutral wind vectors from FPI and WATS data are given by the arrows; measurements of the average exospheric temperature from FPI data are color coded according to scale at right. These data are plotted against angle along the track (see text) and universal time in bins of 5° latitude and 2 hours UT, respectively. The track of the satellite at any given UT is an ascending line through the figure. The bottom half of the figure corresponds to the 2100 hours LT zone and the top half to the 0900 hours LT zone. The wind vectors are plotted with reference to this LT plane with LT increasing in the anticlockwise direction. The white line is the locus of the projection onto the orbit plane of the geomagnetic pole. (*b*) The prediction of the NCAR TGCM model and (*c*) the prediction of the UCL TGCM model are plotted in an identical format.

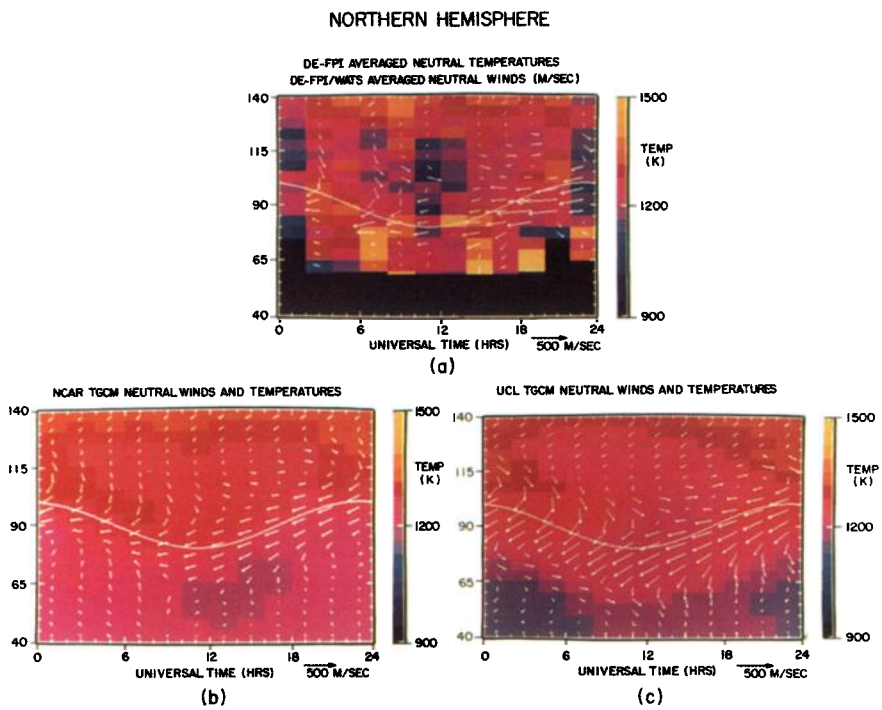

Plate 6. Comparison of the measured and predicted behavior of the thermospheric dynamics and thermodynamics for the winter (north) pole study. (*a*) Measurements of the average neutral wind vectors from FPI and WATS data are given by the arrows; measurements of the average exospheric temperature from FPI data are color coded according to scale at right. These data are plotted against angle along the track (see text) and universal time in bins of 5° latitude and 2 hours UT, respectively. The track of the satellite at any given UT is an ascending line through the figure. The bottom half of the figure corresponds to the 0600 hours LT zone and the top half to the 1800 hours LT zone. The wind vectors are plotted with reference to this LT plane with LT increasing in the anticlockwise direction. The white line is the locus of the projection onto the orbit plane of the geomagnetic pole. (*b*) The prediction of the NCAR TGCM model and (*c*) the prediction of the UCL TGCM model are plotted in an identical format.

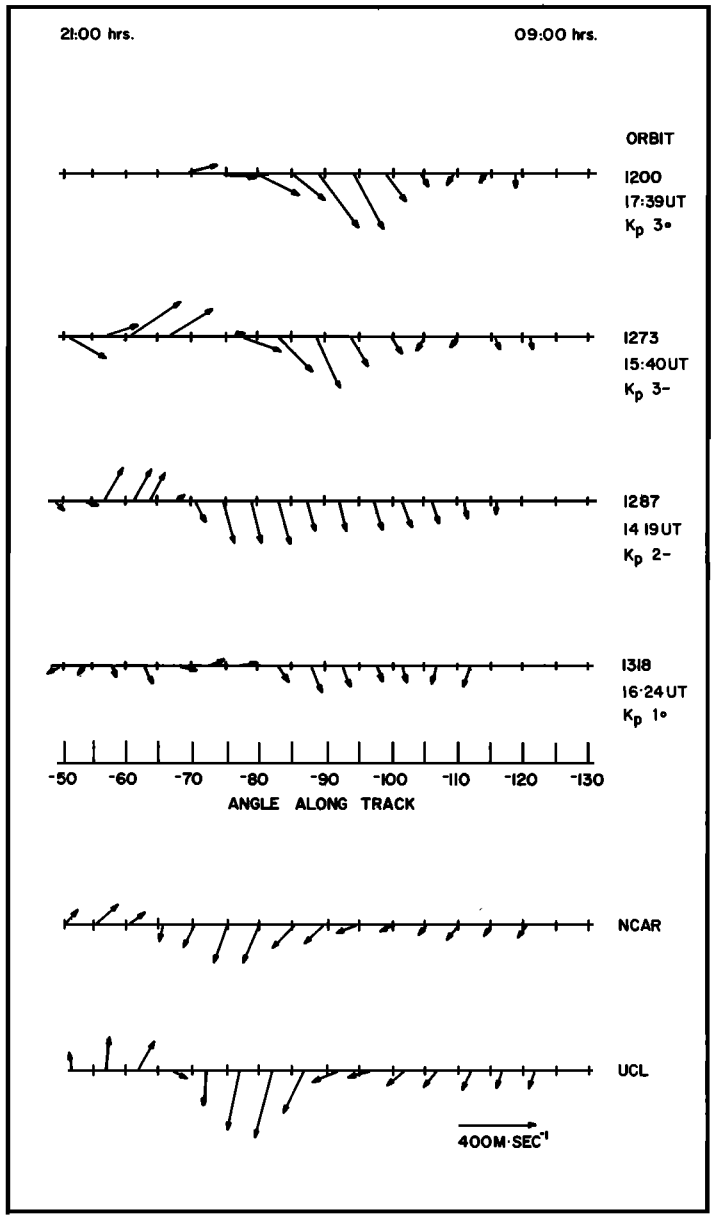

Fig. 4. Neutral wind vectors plotted along the track of DE 2 for four south pole passes from October 1981 at universal times near 1500 hours (top). The satellite crosses the pole from 2100 LT to 0900 LT, and the vectors are plotted with respect to this local time plane (LT increases in anticlockwise direction). Also shown are the model predictions from the NCAR and UCL TGCM's for the same local time plane and universal time conditions (bottom).

is a direct consequence of Joule and soft particle heating in the polar cusp and thermal advection by the polar cap winds.

3. Comparison of Theory With Observations

Through the years there have been many theoretical models of the dynamics of the thermosphere, all of which have their strong and weak points. Most of the previous models adopted time-periodic solutions and various analytic expansions. Recently, finite-difference numerical models have been constructed, and there have been serious attempts to make these models more realistic by incorporating detailed ionospheric models, composition effects, complex ion convection patterns, tilted magnetic poles, improved solar heating efficiency factors, and a multitude of complex feedback effects that cannot be implemented in a simple model. These factors have led to the development of thermospheric general circulation models that can only be run on very large computers [*Fuller-Rowell and Rees*, 1980; *Dickinson et al.*, 1981]. Such large and complex models have the advantage that they represent the physical world in a more realistic way but suffer from the difficulty that they are not easily understood. In fact one must carry out numerical experiments with these models in much the same manner as those we have carried out with the DE instrumentation. We have included on our investigator team representatives of two such modeling efforts: one model being the NCAR TGCM [*Dickinson et al.*, 1981] and the second being the UCL TGCM [*Fuller-Rowell and Rees*, 1980]. Each of these modeling groups was given the conditions under which the DE spacecraft crossed the southern summer pole and the northern winter pole. The resulting numerically derived dynamics fields were then given to the DE experimental team for analysis and display in order to make a direct and meaningful

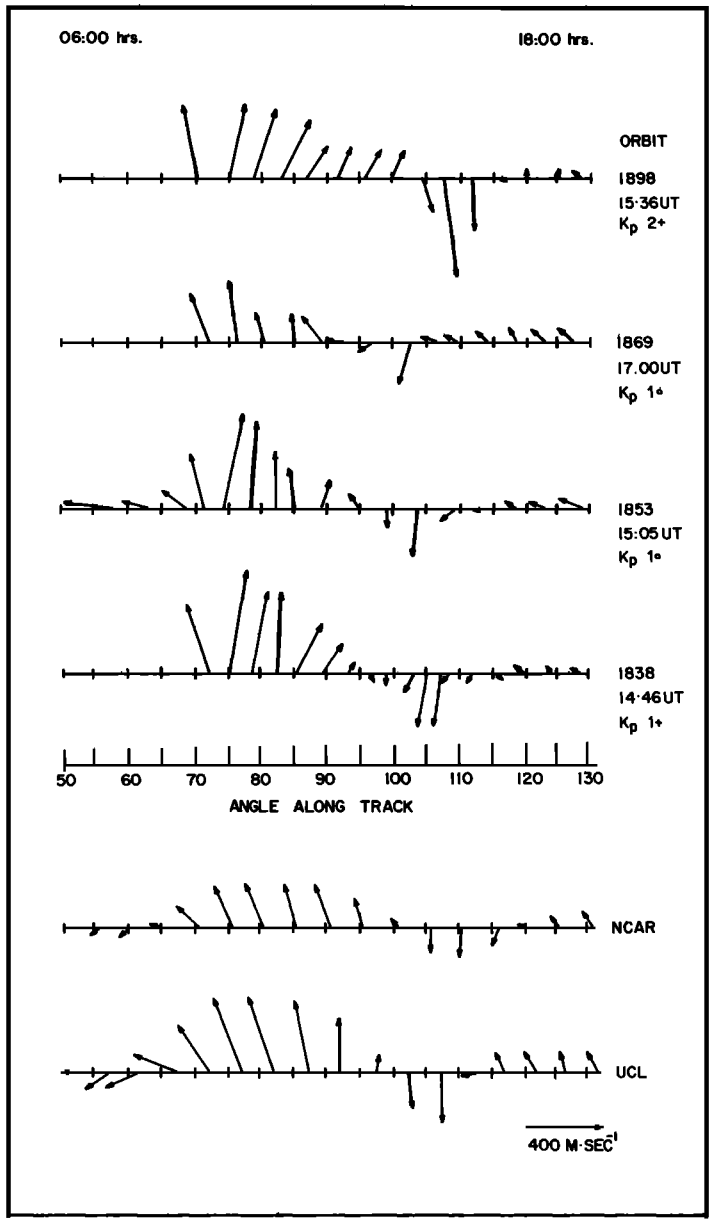

Fig. 5. Neutral wind vectors plotted along the track of DE 2 for four north pole passes from December 1981 at universal times near 1500 hours (top). The satellite crosses the pole from 0600 LT to 1800 LT, and the vectors are plotted with respect to this local time plane (LT increases in anticlockwise direction). Also shown are the model predictions from the NCAR and UCL TGCM's for the same local time plane and universal time conditions (bottom).

comparison between theory and the observational fact. These comparisons are discussed in this section of the paper.

3.1. *Southern Summer Polar Region*

The NCAR and UCL TGCM's were run to equilibrium under input conditions corresponding to the moderate geomagnetic activity that occurred during the period of time when the DE spacecraft was sampling the southern summer polar region (October 13 to November 5, 1982). A detailed description of the input conditions for these model runs is contained in the appendices A and B. We note the difficulty in precisely describing these complex conditions, but we believe that these approximate descriptions will prove useful to the reader. The output of these two models was selected such that the data would simulate the passage of a hypothetical spacecraft along a path identical to that taken by DE.

A graphic example of the comparison of observation and theory is shown in Figure 4, where wind vectors observed on several orbital passes from DE (i.e., orbits 1200, 1273, 1287, and 1318) that occurred near 1500 UT are compared to the thermospheric wind vectors calculated by using the two numerical models. One notes that there are obvious differences between the individual orbits but that there is a strong element of continuity. The trajectory of the spacecraft at 1500 UT is illustrated in Plate 3*c*, where the line representing the sampling volume is seen to pass tangent to the afternoon auroral zone at about 1500 LT. The zonal wind reversal observed near $-120°$ AAT in these individual passes is caused by dayward return ion convection in the early afternoon. This reversal is highly dependent upon the magnitude of the momentum transfer from the ions to the neutral gases of the thermosphere, which itself depends on both the ion drift veloc-

ity and the ion density, both of which are variable. It is also important to recognize that the exact position of the reversal will depend upon the size of the auroral oval, again a variable. We note that, despite these sources of variation, the neutral wind field is relatively stable. The predictions of the two models are shown at the bottom of Figure 4 and demonstrate the same features observed from the spacecraft. The most striking difference between the modeling results and the observations is the difference in the sign of the meridional wind in the region extending from the geographic pole (−90° AAT) and −110° AAT, where the data shows dayward flow and the models show day-to-night flow. This difference may indicate that the ion convection pattern may be considerably more complex than that assumed in the present models.

The comparison of results is completed for the southern summer pole in Plate 5, where 5*a* shows the observational data previously described, 5*b* shows the result of the NCAR TGCM, and 5*c* that of the UCL TGCM. Here we have averaged the experimental results over the October observation period, thus reducing the influence of variable convection and convection pattern size. The general wind vector patterns are similar in all three cases, with variations in the magnitude of the vectors being the dominant apparent difference. There are significant differences in the patterns of the meridional winds that may be related to a lack of realism in the chosen ion convection patterns and the distribution of polar heating used in the models. We are not surprised by the latter, since our understanding of the polar heating is less well developed than the convection velocity pattern. This is also indicated in the temperature fields shown in these maps. It is clear that there are significant differences between the models as well as with the observations in the temperature patterns over the southern magnetic pole, although the hot polar region is shown in all maps.

3.2. *Northern Winter Polar Region*

The NCAR and UCL TGCM were again run to equilibrium under input conditions that, in this case, corresponded to the moderate geomagnetic activity that occurred when the DE spacecraft was sampling the northern winter polar region and crossing the north pole from morning to afternoon (December 2–24, 1982). The input conditions for these model runs are contained in appendices A and B. The output of these two models were again selected such that the data would simulate the passage of a hypothetical spacecraft along a path identical to that taken by DE.

The comparison of observation and theory for this case is shown in Figure 5, where wind vectors observed on several orbital passes from DE (i.e., orbits 1836, 1853, 1869, and 1878) that occurred near 1500 UT are compared to the thermospheric wind vectors calculated by using the two numerical models. The trajectory of the spacecraft over the northern pole at 1500 UT is illustrated in Plate 4*c*, where the path is seen to pass through the midnight sector of the auroral zone at high magnetic latitude, penetrating the auroral zone in the early morning and exiting the oval in the early evening. The reversal in the zonal wind that occurs in the early evening auroral zone is apparent in these data near 110° AAT. This dayward flow is dependent on ion convection and consequently is variable. The transpolar flow over the polar cap is apparent and is a consistent feature of these northern polar passes. The theoretical results are shown at the bottom of Figure 5 and demonstrate many of the same features as the observations. The evening reversal is present in both models, as is the transpolar flow. One interesting difference between the models and the observations is the direction of the transpolar wind. Both models consistently show neutral winds flowing toward about 0200 LT, anticlockwise of the ion convection direction, while the DE winter pole observations show the neutral wind flowing more from midday to midnight, close to the expected ion flow direction. This factor may be due to the polar ionosphere being enhanced by particle precipitation to a larger extent than the theoretical ionospheres embedded within the TGCM's.

The northern winter winds are more fully examined in Plate 6, where 6*a* shows the observational data previously described, 6*b* shows the result of the NCAR TGCM, and 6*c* shows that of the UCL TGCM. Here again we have averaged the experimental results over the observation period, thus reducing the influence of variable convection and convection pattern size. The general wind vector patterns are similar in all three cases, with variations in the magnitude and direction of the transpolar wind being the dominant apparent difference. The main differences between the observations and calculations occur in the temperature fields. The observed temperatures in the winter polar region are larger than model predictions, and in particular the observed temperature variations are considerably larger than either model prediction. Neither model predicts the cold temperature region on the evening side of the auroral oval near 0100 and 1300 UT. The observed temperature difference between the magnetic pole and evening auroral oval is about 300 K at 1300 UT. This cold region may be the result of a dynamic or compositional adjustment to the intense ion convection on the evening side of the auroral oval or a consequence of transport from the night to the dayside. In a similar manner the winter polar cap may be generally cold, and the temperature in the polar cap may be enhanced by thermal advection from the polar cusp and dayside ionosphere. This feature requires further investigation when the models include the appropriate coupling with composition.

4. SUMMARY

This paper has described the observations of the thermospheric wind fields observed from the Dynamics Explorer 2 spacecraft during perigee transits of the southern summer pole and the northern winter pole. A primary conclusion of the study of these data is that above 60 degrees of latitude the neutral winds in the upper thermosphere are most sensibly ordered in a coordinate system attached to the magnetic poles. The physical reason for this fact is that the thermospheric wind system responds primarily to magnetospheric forcing mapped into the auroral regions surrounding the magnetic poles of the earth. This magnetospheric forcing is manifest in three forms: one being the momentum transfer between convecting ions and the neutral gases of the atmosphere; the second being the Joule heating of the neutrals, which results from dissipation of energy between the convecting ions and the neutral atmosphere; and the third is the direct injection of energy as a result of the precipitation of low-energy particles into the atmosphere. Of these factors, momentum transfer has the most direct influence on the neutral atmospheric winds, while the Joule heating and low-energy particle precipitation have a dominant influence on the temperature of the high thermosphere.

Comparison of the observed dynamic and thermodynamic fields with two of the existing thermospheric general circulation models indicate some areas of agreement and some areas of disagreement. There is general agreement between the

model calculations and observations indicating an enhanced antisunward flow over the magnetic polar cap and a sunward flow in the vicinity of the auroral zone. There are, however, differences in the magnitude of the observed winds and in the boundary locations of the regions of enhanced wind flow from those calculated in both models. These differences are most likely due to differences in the actual ion drag momentum source from that used in the model parameterizations. The ion drag momentum source is governed by both the ion drift pattern and the electron density. The NCAR-TGCM used the simplified *Volland* [1975] model as modified by *Sojka et al.* [1979, 1980] and arbitrarily assumed a 60-kV cross-tail potential to represent the average geophysical conditions appropriate to the measurements. The electron density was specified by the *Chiu* [1975] empirical model. The UCL-TGCM used the ion convection model of *Quegan et al.* [1982] with a specified global magnetospheric energy input of 8×10^{12} W. The differences in the winds calculated by the two models are due to differences in model inputs. Better agreement with observations in both models could be made by an appropriate adjustment of input parameters. This, however, was not attempted while awaiting a better prescription of the ion drag forcing derived from the Dynamics Explorer satellite by using data taken at the same time the wind measurements are made.

There are clearly first-order differences between the observed and predicted temperature fields. Both models fail to exhibit the increase in polar cap temperature observed in the northern winter and do not show the deep minimum in the evening auroral oval. Two primary factors may be responsible for this lack of agreement: first, there is a large uncertainty in the low-energy electron precipitation in the polar cusp, and these particles deposit their energy at high altitudes, where the temperature enhancement is observed; second, the influence of compositional coupling has not been accurately introduced into the models. In addition to these direct influences there is also the fact that we are observing a dynamic process that is responding to temporally varying energy inputs. Auroral substorms and larger-scale variations associated with magnetic storms are being smoothed in our averaging of the observed winds and temperatures, while the theories are treating the process for these simulations as steady state.

The outcome of this study indicates that the thermosphere is a region of great variability, exhibiting a climatology as complex as that of the lower atmosphere on which it rests. There is a reasonable theoretical foundation on which to build an understanding of this atmospheric system, but this theoretical structure needs to be further developed. First-order forcing functions for the models are in a rather rudimentary state and must be improved before significant point-by-point comparisons can be carried out.

APPENDIX A

The NCAR Thermospheric General Circulation Model

The NCAR thermospheric general circulation model (TGCM) used to calcualte the UT variation of winds and temperature along the DE 2 satellite track has been described in detail by *Dickinson et al.* [1981] and by *Roble et al.* [1982]. Various parameterized inputs used in the model have been discussed previously by *Dickinson et al.* [1975, 1977, 1981, 1983] and *Roble et al.* [1977, 1982, 1983]. The time-dependent model has a 5° latitude-by-longitude grid with 24 constant pressure surface layers in the vertical extending from approximately 97-km to 500-km altitude. The solar EUV heating rates are calculated by using the solar flux values of *Hinteregger* [1981] (F10.7 near 200) and absorption cross sections specified by *Torr et al.* [1979] and the neutral gas heating efficiency parameterization by B. A. Emery (private communication, 1982). The global mean neutral gas temperature and global distribution of composition are specified by the mass spectrometer and incoherent scatter (MSIS) empirical model [*Hedin et al.*, 1977*a*, *b*]. The ion drag tensor is determined from the empirical model of electron density of *Chiu* [1975]. Both the composition and ion drag tensor are assumed to remain fixed in local time as the earth rotates. For the model calculations the cross-tail potential of the *Sojka et al.* [1980] ion convection model is arbitrarily set to 60 kV and the TGCM is run for five model days or until a diurnally reproducible pattern is obtained. A history tape is written containing the global distribution of winds and temperatures for each hour UT, and a processing code is then used to determine the zonal and meridional wind components and temperature along the track of the DE 2 satellite track at a given UT.

Other input parameterizations used for the NCAR TGCM calculations are summarized below.

Input Parameters Used in the NCAR TGCM Calculations

Geomagnetic input. Magnetospheric convection model of *Volland* [1978] as modified by *Sojka et al.* [1979, 1980]. The magnetospheric convection pattern is sun-aligned relative to the geomagnetic poles (north geomagnetic pole 78.3°N latitude and 291°E longitude, south geomagnetic pole 74.5°S latitude and 127.0°E longitude), so corotation of ionospheric plasma is included in the TGCM coordinate system that rotates with the earth. Only Joule heating and ion drag momentum sources resulting from the relative drift between the ions and the neutrals are considered. There is no heating or ion drag enhancement because of auroral particle precipitation considered for the calculations. The cross-tail potential for the magnetospheric convection model is assumed to be 60 kV, giving ion drift velocities typically 500 m s^{-1} in the antisunward direction over the polar cap, with about 1 km s^{-1} in a narrow sunward convection channel near the auroral zone.

Solar EUV/UV heating. (1) October 23, 1981, for southern hemisphere polar passes; (2) December 4, 1981, for northern hemisphere polar passes; solar activity $F10.7 = 200 \times 10^{-22}$ W m^{-2} Hz^{-1}

Total energy input. Global solar EUV/UV, 10^{12} W; global Joule heating, 8×10^{10} W; summer/winter Joule heating ratio, 3; auroral particle precipitation heating, 0 W.

APPENDIX B

The UCL Thermospheric General Circulation Model

The formulation and numerical procedures of the University College London (UCL) three-dimensional, time-dependent model have been described in a series of papers [*Fuller-Rowell and Rees*, 1980, 1981; *Rees et al.*, 1980]. The model is mainly intended to simulate the dynamical structure of the thermosphere above about 100-km altitude.

A global grid 2° latitude by 18° longitude is used that rotates with the earth. Seventeen pressure levels represent the vertical variation of the atmosphere between 80 km (isopycnic level) and about 500 km at mean solar activity. The solar EUV and UV fluxes of *Hinteregger* [1981] and *Torr et al.* [1980] are used together with the heating efficiencies derived from *Torr et al.* [1980, 1981]. The solar input has a realistic local time and seasonal/latitudinal structure so that the sea-

sonal and solar activity variations can be independently determined.

The "geomagnetic" input is derived from models of the momentum and energy transferred via the earth's magnetic field from the solar wind/magnetospheric dynamo to the high-latitude ionosphere and thermosphere. A semiempirical electric field model based on the work of *Quegan et al.* [1982] has been used for the simulations presented in this paper. The input parameters to the UCL TGCM runs presented here are summarized below.

Input Parameters Used in the UCL TGCM Calculations

Geomagnetic input. "Sheffield" high-latitude ionospheric model (>60° geomagnetic latitude) adapted from *Quegan et al.* [1982]. No additional high-latitude particle heating/ionization source at high latitude; in particular, no *E* region ionization enhancement such as would occur in a substorm. The direct energy deposited by the cusp and auroral oval precipitation used in the Sheffield ionosphere is not included in the energy equation. Joule heating is included, calculated locally from the differential ion/neutral drift velocity, the local electric field, and the local electron densities.

Solar EUV/UV heating. (1) October 16, 1981 (solar declination −9°); (2) December 21, 1981 (solar declination −23°); solar activity F10.7 = 150×10^{-22} Wm^{-2} Hz^{-1}.

Total energy input. Global solar EUV/UV, 10^{12} W; global magnetospheric, 8×10^{10} W; global particles (<200 eV), 0.5–1 ergs cm^2 s $\times 10^{10}$; summer/winter UT average December 21, 2.5:1; magnetospheric input ratio UT average October 16?, 2:1.

Acknowledgments. The Editor thanks J. M. Straus and M. F. Larsen for their assistance in evaluating this paper. The National Center for Atmospheric Research is sponsored by the National Science Foundation.

REFERENCES

Chiu, Y. T., An improved phenomenological model of ionospheric density, *J. Atmos. Terr. Phys.*, *37*, 1563–1570, 1975.

DeVries, L. L., Structure and motion of the thermosphere shown by density data from the Low-G Accelerometer Calibration System (LOGACS), *Space Res.*, *12*, 867–879, 1972.

Dickinson, R. E., R. G. Roble, and E. C. Ridley, Response of the neutral thermosphere at *F* region heights to interaction of a global wind with anomalies of ionization, *J. Atmos. Sci.*, *28*, 1280, 1971.

Dickinson, R. E., E. C. Ridley, and R. G. Roble, Meridional circulation in the thermosphere, 1, Equinox conditions, *J. Atmos. Sci.*, *32*, 1737–1754, 1975.

Dickinson, R. E., E. C. Ridley, and R. G. Roble, Meridional circulation in the thermosphere, 2, Solstice conditions, *J. Atmos. Sci.*, *34*, 178–192, 1977.

Dickinson, R. E., E. C. Ridley, and R. G. Roble, A three-dimensional general circulation model of the thermosphere, *J. Geophys. Res.*, *86*, 1499–1512, 1981.

Dickinson, R. E., E. C. Ridley, and R. G. Roble, Thermospheric general circulation with coupled dynamics and composition, *J. Atmos. Sci.*, in press, 1983.

Fedder, J. A., and P. M. Banks, Convection electric fields and polar thermospheric winds, *J. Geophys. Res.*, *77*, 2328, 1972.

Frank, L. A., J. D. Craven, K. L. Ackerson, M. R. English, R. H. Eather, and R. L. Carovillano, Global auroral imaging instrumentation for the Dynamics Explorer mission, *Space. Sci. Instrum.*, *5*, 369–393, 1981.

Fuller-Rowell, T. J., and D. Rees, A three-dimensional time-dependent global model of the thermosphere, *J. Atmos. Sci.*, *37*, 2545–2567, 1980.

Fuller-Rowell, T. J., and D. Rees, A three-dimensional time-dependent simulation of the global dynamical response of the thermospheric to a geomagnetic substorm, *J. Atmos. Terr. Phys.*, *43*, 701–721, 1981.

Hays, P. B., R. A. Jones, and M. H. Rees, Auroral heating and the composition of the neutral atmosphere, *Planet. Space Sci.*, *21*, 559–573, 1973.

Hays, P. B., J. W. Meriwether, and R. G. Roble, Nighttime thermospheric winds at high latitudes, *J. Geophys. Res.*, *84*, 1905–1913, 1979.

Hays, P. B., T. L. Killeen, and B. C. Kennedy, The Fabry-Perot interferometer on Dynamics Explorer, *Space Sci. Instrum.*, *5*, 395–416, 1981.

Hedin, A. E., et al., A global thermospheric model based on mass spectrometer and incoherent scatter data, MSIS, 1, N_2 density and temperature, *J. Geophys. Res.*, *82*, 2139–2147, 1977*a*.

Hedin, A. E., C. A. Reber, G. P. Newton, N. W. Spencer, H. C. Brinton, H. G. Mayr, and W. E. Potter, A global thermospheric model based on mass spectrometer and incoherent scatter data, MSIS, 2, Composition, *J. Geophys. Res.*, *82*, 2148–2156, 1977*b*.

Heppner, J. P., Empirical models of high-latitude electric fields, *J. Geophys. Res.*, *82*, 1115–1125, 1977.

Hinteregger, H. E., Representations of solar EUV fluxes for aeronomical applications, *Adv. Space Res.*, *1*, 39–52, 1981.

Hoffman, R. A., G. D. Hogan, and R. C. Maehl, Dynamics Explorer spacecraft and ground operations systems, *Space Sci. Instrum.*, *5*, 349–367, 1981.

Kelley, M. C., T. S. Jorgensen, and I. S. Mikkelsen, Thermospheric wind measurements in the polar region, *J. Atmos. Terr. Phys.*, *39*, 211, 1977.

Killeen, T. L., P. B. Hays, N. W. Spencer, L. E. Wharton, Neutral winds in the polar thermosphere as measured from Dynamic Explorer, *Geophys. Res. Lett.*, *9*, 957–960, 1982.

Killeen, T. L., P. B. Hays, N. W. Spencer, L. E. Wharton, Neutral winds in the polar thermosphere as measured from Dynamics Explorer, *Adv. Space Res.*, *2*, 133–136, 1983.

Mayr, H. G., and I. Harris, Some characteristics of electric field momentum coupling with the neutral atmosphere, *J. Geophys. Res.*, *83*, 3327–3336, 1978.

Mayr, H. G., and I. Harris, *F* region dynamics, *Rev. Geophys. Space Phys.*, *17*, 492–509, 1979.

Mayr, H. G., I. Harris, N. W. Spencer, Some properties of upper atmosphere dynamics, *Rev. Geophys. Space Phys.*, *16*, 539–565, 1978.

Meriwether, J. W., J. P. Heppner, J. D. Stolarik, and E. M. Wescott, Neutral winds above 200 km at high latitudes, *J. Geophys. Res.*, *78*, 6643–6661, 1973.

Nagy, A. F., R. J. Cicerone, P. B. Hays, K. D. McWatters, J. W. Meriwether, A. E. Belon, and C. L. Rino, Simultaneous measurement of ion and neutral motions by radar and optical techniques, *Radio Sci.*, *9*, 315–321, 1974.

Quegan, S., G. J. Bailey, R. J. Moffett, R. A. Heelis, T. J. Fuller-Rowell, D. Rees and R. W. Spiro, A theoretical study of the distribution of ionization in the high latitude ionosphere and plasmasphere: First results on the mid-latitude trough and the light-ion trough, *J. Atmos. Terr. Phys.*, *44*, 619–640, 1982.

Rees, D., T. J. Fuller-Rowell, R. W. Smith, Measurements of high latitude thermospheric winds by rocket and ground-based techniques and their interpretation using a three-dimensional time-dependent dynamical model, *Planet. Space Sci.*, *28*, 919–932, 1980.

Rishbeth, H., Thermospheric winds and the *F* region, A review, *J. Atmos. Terr. Phys.*, *34*, 1–47, 1972.

Rishbeth, H., Dynamics of the equatorial *F* region, *J. Atmos. Terr. Phys.*, *39*, 1159–1168, 1977.

Rishbeth, H., Ion drag effects in the thermosphere, *J. Atmos. Terr. Phys.*, *41*, 885–894, 1979.

Rishbeth, H., and W. B. Hanson, A comment on plasma "pile-up" in the *F* region, *J. Atmos. Terr. Phys.*, *36*, 703–706, 1974.

Roble, R. G., Dynamics of the earth's thermosphere, *Rev. Geophys. Space Phys.*, in press, 1983.

Roble, R. G., R. E. Dickinson, and E. C. Ridley, Seasonal and solar cycle variations of the zonal mean circulation in the thermosphere, *J. Geophys. Res.*, *84*, 5493–5504, 1977.

Roble, R. G., R. E. Dickinson, and E. C. Ridley, Global circulation and temperature structure of thermosphere with high-latitude plasma convection, *J. Geophys. Res.*, *87*, 1599–1614, 1982.

Roble, R. G., R. E. Dickinson, E. C. Ridley, B. A. Emery, P. B. Hays, T. L. Killeen, and N. W. Spencer, The high latitude circulation and temperature structure of the thermosphere near solstice, *Planet. Space Sci.*, *31*, 1299–1314, 1983.

Rothwell, P., R. Mountford, and G. Martelli, Neutral wind modifications above 150 km altitude associated with the polar substorm,

J. Atmos. Terr. Phys., 36, 1915–1926, 1974.
Sojka, J. J., W. J. Raitt, and R. W. Schunk, Effect of displaced geomagnetic and geographic poles on high-latitude plasma convection and ionospheric depletions, *J. Geophys. Res., 84*, 5943–5951, 1979.
Sojka, J. J., W. J. Raitt, and R. W. Schunk, A comparison of model predictions for plasma convection in the northern and southern polar regions, *J. Geophys. Res., 85*, 1762–1768, 1980.
Spencer, N. W., L. E. Wharton, H. B. Niemann, A. E. Hedin, G. R. Carignan, J. C. Maurer, The Dynamics Explorer wind and temperature spectrometer, *Space Sci. Instrum., 5*, 417–428, 1981.
Spencer, N. W., L. E. Wharton, G. R. Carignan, J. C. Maurer, Thermosphere zonal winds, vertical motions, and temperature as measured from Dynamics Explorer, *Geophys. Res. Lett., 9*, 953–956, 1982.
Straus, J. M., Dynamics of the thermosphere at high latitudes, *Rev. Geophys. Space Phys., 16*, 183–194, 1978.
Stoffregen, W., Anomaly of the neutral wind at 200 km height at high latitudes, in *Magnetosphere-Ionosphere Interactions*, edited by K. Kolkstead, Unversitetsponlaget, Oslo, Norway, 1972.
Torr, M. R., D. G. Torr, R. A. Ong, and H. E. Hinteregger, Ionization frequencies for major thermospheric constituents as a function of solar cycle 21, *Geophys. Res. Lett., 10*, 771–774, 1979.
Torr, M. R., D. G. Torr, and P. G. Richards, The solar ultraviolet heating efficiency of the mid-latitude thermosphere, *Geophys. Res. Lett., 7*, 373–376, 1980.
Torr, M. R., P. G. Richards, and D. G. Torr, A new determination of the ultraviolet heating efficiency of the thermosphere, *J. Geophys. Res., 85*, 6819–6826, 1981.
Volland H., Magnetospheric electric fields and currents and their influence on large scale thermospheric circulation and composition, *J. Atmos. Terr. Phys., 41*, 853–866, 1979.
Wu, S. T., S. Matsushita, and L. L. DeVries, An analysis of the upper atmospheric wind observed by LOGACS, *Planet. Space Sci., 22*, 1036, 1974.

J. D. Craven and L. A. Frank, Department of Physics and Astronomy, University of Iowa, Iowa City, IA 52242.
B. A. Emery and R. G. Roble, National Center for Atmospheric Research, Boulder, CO 80307.
T. J. Fuller-Rowell and D. Rees, Department of Physics and Astronomy, University College London, London, England.
P. B. Hays and T. L. Killeen, Space Physics Research Laboratory, The University of Michigan, Ann Arbor, MI 48109.
N. W. Spencer and L. E. Wharton, Goddard Space Flight Center, National Aeronautics and Space Administration, Greenbelt, MD 20771.

(Received May 16, 1983;
revised January 11, 1984;
accepted January 23, 1984.)